Constitutive Immune Activity Promotes Tumorigenesis in *Drosophila* Intestinal Progenitor Cells.

Kristina Petkau, Silvia Guntermann, Edan Foley*.

Department of Medical Microbiology and Immunology

Institute of Virology

University of Alberta

Edmonton, Alberta

Canada.

*Corresponding author.

Email: efoley@ualberta.ca

SUMMARY

The endoderm is a critical first point of contact between a host and their immediate environment. Gut innate immune defenses contain bacterial populations and protect the host interior from invasive microbes. Although excess intestinal immune activity frequently promotes inflammatory illnesses, we know very little about the consequences of chronic innate immune activity exclusively in endodermal gut cells of an otherwise normal animal. To address this question, we generated a transgenic line that allows us to activate inflammatory signals in fly intestinal progenitor cells. We found that constitutive immune activity in intestinal progenitors disrupts expression of homeostatic regulators such as Notch signal transduction pathway components and induces hyperplasia throughout the gut. Consistent with links between immune activity and the Notch pathway, we showed that persistent immune signaling interferes with progenitor cell differentiation and exacerbates the formation of Notch-dependent intestinal tumors. These findings uncover a novel link between constitutive immune activity and tumorigenesis in intestinal stem cells.

INTRODUCTION

Endodermal tissues are at the heart of an ancient, intimate, and continuous relationship between multicellular organisms and the microbial world. Gut commensal bacteria negotiate a semi-stable existence within host niches, partially through provision of factors that influence nutrition, development, and immunity in the host (Cho and Blaser, 2012). For their part, hosts invest substantial amounts of energy and resources in the containment of intestinal microbes (Hooper et al., 2012). Physical barriers such as the peritrophic matrix of insects, or dense mucosal layers of mammals, keep microbes at an adequate distance from gut cells. Additionally, host-derived reactive oxygen and nitrogen species destroy invading microbes, while antimicrobial effectors block microbial dissemination throughout the host.

The consequences of failed antibacterial defenses are often extreme, and occasionally deadly for the host. For example, dysbiotic microbial communities contribute to traumatic inflammatory bowel diseases in humans (Wlodarska et al., 2015). In recent years, we have made considerable advances in relationships between adaptive immune responses and gut microbiota (Honda and Littman, 2016). Although these studies have an immediate biomedical relevance, it is important to remember that adaptive immunity is an evolutionary newcomer that is restricted to a small fraction of extant animal species. Most animals rely exclusively on innate immune systems to manage contacts with microbes, and innate signals direct adaptive immune responses in vertebrates. Innate defenses are particularly significant in the endoderm, the primary site of contact between multicellular organisms and their immediate microbial environment. Despite the importance of endodermal innate immunity for the restraint of gut microbes, very few

studies examine the consequences of deregulated innate immune activity specifically in endodermal gut cells of an otherwise wild-type animal.

The fruit fly, *Drosophila melanogaster*, is an ideal model for the characterization of intestinal development and function (Buchon et al., 2013, Jiang and Edgar, 2012, Lemaitre and Miguel-Aliaga, 2013). For example, studies with *Drosophila* provided foundational insights into Notch-mediated regulation of gut development (Guo and Ohlstein, 2015, Micchelli and Perrimon, 2006, Ohlstein and Spradling, 2006, Ohlstein and Spradling, 2007), and intestinal tumorigenesis (Patel and Edgar, 2014, Biteau and Jasper, 2011, Marianes and Spradling, 2013, Apidianakis et al., 2009). In the fly midgut, basal intestinal stem cells (ISC) divide to generate a bipotent transient cell type, the enteroblast (EB). Delta-Notch signals between ISC-EB progenitor cell pairs determines the developmental fate of EBs (Takashima et al., 2011, Perdigoto et al., 2011). High levels of Notch activity in enteroblasts lead to their differentiation as large, polyploid, absorptive enterocytes (EC). Lower levels of Notch activity result in the differentiation of enteroblasts as smaller, diploid, secretory enteroendocrine cells (EE). Notch-dependent control of progenitor cell differentiation is conserved across vast evolutionary distances, with similar requirements in species as diverse as fish and rodents (Fre et al., 2005, Stanger et al., 2005, van Es et al., 2005, Crosnier et al., 2005), and interruptions to Notch signaling lead to intestinal tumor formation in several models (Kazanjian and Shroyer, 2011, Peignon et al., 2011).

Fly intestinal immunity relies exclusively on the immune deficiency (IMD) pathway (Buchon et al., 2009, Lhocine et al., 2008), a defense response with similarities to the mammalian tumor necrosis factor (TNF) cascade (Buchon et al., 2014). In the fly, detection of bacterial peptidoglycan results in the proteolytic removal of thirty N-terminal amino acids from the Imd adaptor protein by the

caspase Dredd (Paquette et al., 2010). Cleaved Imd associates with the Inhibitor of Apoptosis 2 (IAP2) and Fas-Associated Death Domain (FADD) orthologs (Guntermann and Foley, 2011, Paquette et al., 2010) to activate the NF-kB transcription factor Relish (Dushay et al., 1996). Active Relish relocates to the nucleus and initiates transcription of a broad spectrum of antimicrobial effectors. Early studies of IMD pathway function focused on Relish-dependent induction of antimicrobial peptides. However, recent work showed that intestinal IMD activity also controls the expression of genes involved in developmental and metabolic processes (Broderick et al., 2014, Erkosar et al., 2014). These studies hint at novel, unstudied biological roles for IMD that extend beyond the extermination of unwanted bacteria.

Despite the prominent role of IMD in the control of innate immunity, we know little about the effects of constitutive intestinal IMD activity in an adult. To address this, we engineered a novel IMD variant that permits temporal and tissue-specific activation of IMD. We used this line to characterize the consequences of persistent IMD activity in fly midgut progenitor cells. Our studies uncovered an unanticipated impact of IMD on progenitor cell differentiation. We showed that constitutive immune signaling altered the expression of Notch pathway regulators, disturbed EE differentiation, and caused hyperplasia throughout the posterior midgut. Consistent with interactions between IMD and Notch, we found that constitutive IMD activity greatly exacerbated the formation of Notch-dependent tumors. Given the involvement of Notch signaling in vertebrate intestinal tumor development, we believe our findings may be of particular relevance to studies that explore relationships between intestinal inflammation and tumorigenesis.

RESULTS

Constitutive IMD Pathway Activation in Intestinal Stem Cells.

To characterize the effects of constitutive immune signaling in the intestine, we generated a transgenic *Drosophila* line that allows cell-restricted activation of the IMD pathway. Specifically, we engineered a truncated IMD protein that uses an internal ATG (at residue 78) as a start codon. We refer to this truncated protein as ImdCA. ImdCA lacks inhibitory N-terminal amino acids (Figure 1A), but retains the ability to interact with the FADD adaptor protein (Figure 1B). We generated transgenic fly lines that permit temperature-dependent expression of ImdCA in fat tissue (*cgGAL4* ; *GAL80^{ts}/UASimdCA* (abbreviated as *cg^{ts}>CA*)), or ISC/EB progenitor cell pairs (*esgGAL4*, *GAL80^{ts}*, *UASGFP* ; *UASimdCA* (abbreviated as *esg^{ts}>CA*)). Incubation of either genotype at 29°C, the restrictive temperature for *GAL80^{ts}*, results in tissue-specific expression of ImdCA in fat body or intestinal progenitor cells, respectively. In the fat body, the principle site of humoral immunity, ImdCA caused expression of the IMD-responsive antimicrobial peptides *dpt* and *att* (Figure 1C). The induction of *dpt* and *att* proceeded via a classical IMD response, as null mutations in *dredd* prevented ImdCA-mediated antimicrobial peptide expression (Figure 1D). ImdCA is equally effective at inducing antimicrobial expression in midgut progenitor cells (Figure 1E), and expression of ImdCA provided protective benefits against lethal challenges with the gastrointestinal pathogen *Vibrio cholerae* (Figure 1F). These data show that we have established a novel fly line that permits tissue-specific activation of IMD responses in *Drosophila*.

A Balance of Microbial Cues and Host Immune Status Determines Gene Expression Patterns in the Adult Midgut.

To characterize the effects of ImdCA expression in intestinal progenitors, we prepared transcriptional profiles of the intestines of *esg*^{ts} and *esg*^{ts}*>CA* adult flies that we raised at 18°C for ten days, and shifted to 29°C for two days. We examined *esg*^{ts} or *esg*^{ts}*>CA* flies raised under conventional or germ-free conditions in these studies. This experimental strategy allowed us to make pairwise comparisons of the effects of commensal bacteria and ImdCA on the control of host transcription (Figure 2A-D). Similar to earlier studies (Broderick et al., 2014, Erkosar et al., 2014), we found that the microbiome regulates the expression a large cohort of host genes, with a particularly notable effect on genes involved in metabolic processes (Figure 2A-D, Figure S1, E-F, Table S1). As expected, ImdCA altered the expression of genes with known roles in innate defenses. However, we also noticed effects of ImdCA on pathways as diverse as metabolism, transportation and stress responses (Figures 2, 3).

Comparisons between the individual expression profiles uncovered substantial effects of the microbiome on ImdCA-regulated transcription. For example, only 39 of the 212 host genes upregulated in response to ImdCA are induced in conventionally-reared and germ-free animals (Figure 3E). In contrast, 152 transcripts are only induced in the presence of an intact microbiome, and an additional 21 transcripts are only induced in the absence of a microbiome (Figure 3E). Likewise, microbiome-response genes are heavily influenced by the extent of immune activity in the gut. For example, a unique set of 130 genes responds to presence of the microbiome only upon induction of ImdCA (Figure 3F). GO term analysis showed that the microbiome and immune activity synergistically influence functional outputs in the gut. For example, ImdCA only promotes protein glycosylation in the presence of a microbiome (Figure 2E), and the gut microbiome induces tricarboxylic acid cycle genes only when accompanied by intestinal inflammation (Figure

2F). Combined, these data show that gut transcriptional outputs reflect the extent of immune activity and microbial presence in the gut.

Given the effects of ImdCA on antimicrobial peptide expression, we assumed that ImdCA will affect composition of the host microbiome. To test this, we treated freshly eclosed *esg*^{ts} and *esg*^{ts}*>CA* flies with a regime of antibiotics for six days to eliminate the endogenous microbiome. We then fed all flies a homogenate prepared from our lab wild-type *Drosophila* strain, and passaged flies to fresh food twice over seven days to facilitate stable association between microbes in the homogenate and the recipient flies. After seven days, we shifted recipients to 29°C for an additional seven days to activate the IMD pathway in *esg*^{ts}*>CA* flies. We dissected the intestines of the different populations and used deep-sequencing of 16S DNA to identify the microbial communities present in the respective guts (Figure 4). As expected, the microbiome of *esg*^{ts} flies was barely distinguishable from the homogenate. Both microbiomes contained a limited number of OTUs characterized primarily by *Acetobacter* and *Lactobacilli* (Figure 4). Contrary to our initial expectation, we did not observe a notable impact of ImdCA on microbiome composition. In fact, the microbiomes of the original homogenate, the *esg*^{ts} flies, and the *esg*^{ts}*>CA* flies were barely distinguishable (Figure 4), suggesting that the *Drosophila* microbiome is relatively insensitive to elevated IMD pathway activity.

Constitutive IMD Pathway Activation Causes Dysplasia in Intestinal Stem Cells.

In contrast to the minimal effects on the microbiome, we noticed that ImdCA affected expression of several regulators of intestinal homeostasis. This included elements of Wnt, Ras, Insulin, JNK and JAK/STAT pathways (Figure 5A). This observation led us to ask if ImdCA impacts

intestinal morphology. To address this question, we examined the posterior midguts of two and twenty-six day old *esg*^{ts}*>CA* and control *esg*^{ts} flies. We found that acute activation of the IMD pathway had little to no effect on midgut architecture. The posterior midguts of two-day old *esg*^{ts} and *esg*^{ts}*>CA* flies raised at 29°C were essentially indistinguishable (Figure 6 A-H). In both cases, anti-Armadillo (beta-catenin ortholog) immunofluorescence showed a regular arrangement of large, polyploid ECs, that were interspersed with small, Prospero positive EE cells (Figure 6 A, E). Likewise, the posterior midguts of both genotypes contained regularly spaced nuclei (Figure 6 B, F) and evenly distributed GFP positive progenitor cells (Figure 6 C, G).

By 26 days, the posterior midguts of control *esg*^{ts} flies displayed classical hallmarks of age-dependent dysplasia such as a disorganized epithelium (Figure 6 I), uneven arrangements of nuclei (Figure 3 J), and irregular patterns of GFP expression (Figure 6 K-L, and R). We noticed that midgut architecture was further disrupted in 26 day-old *esg*^{ts}*>CA* flies. In this case, we detected a near complete breakdown of epithelial organization (Figure 6M), an increase in cell density (Figure 6N, 4E), and an increase in GFP positive cells (Figure 6 O-P and S).

Given the enhanced dysplasia and altered expression of homeostatic regulators in older *esg*^{ts}*>CA* flies, we reasoned that ImdCA affects proliferation rates in intestinal progenitor cells. To test this hypothesis, we used anti-phosphorylated histone H3 immunofluorescence to count mitotic cells in the intestines of fourteen and twenty-four day-old *esg*^{ts} and *esg*^{ts}*>CA* files. At both ages, we detected a significant increase in mitotic events in *esg*^{ts}*>CA* intestines relative to age-matched *esg*^{ts} controls (Figure 6T). These data show that persistent expression of ImdCA in adult midgut progenitor cells disrupts expression of homeostatic regulators, increases cell proliferation, and promotes tissue hyperplasia.

Persistent IMD Signals Disrupt Notch Activity.

Among homeostatic regulators, ImdCA had a pronounced effect on expression of Notch pathway components (Figure 5B). This observation matches an earlier report of deregulated expression of Notch pathway genes in *imd* mutant flies (Broderick et al., 2014), and raises the possibility that the IMD pathway influences Notch activity in the adult. To test if ImdCA affects progenitor cell differentiation, we used MARCM analysis to identify individual mitoses and subsequent differentiation events in adult posterior midguts. As expected, mitotic clones in conventional flies contained a mix of smaller cells (most likely progenitors and EE), and larger, polyploid ECs (Figure 5 C – F). In contrast, we rarely detected large, polyploid cells in mitotic clones that express ImdCA. Instead, ImdCA clones typically contained aggregates of small cells (Figure 5 G – J). These observations suggest that persistent expression of ImdCA in progenitor cells affects the differentiation of EBs into ECs.

To directly test the possibility that ImdCA disturbs EB differentiation, we counted the numbers of EE cells in the intestines of twenty-four days old esg^{ts} and esg^{ts}*>CA* flies. As expected, the posterior midguts of esg^{ts}*>CA* flies contained greater numbers of cells per area than those observed in age-matched, control esg^{ts} flies (Figure 7 A, D, G). However, we also found that a significantly greater percentage of midgut cells expressed the EE marker Prospero in esg^{ts}*>CA* than in esg^{ts} midguts (Figure 7 B, E, H). These data show that persistent expression of ImdCA disrupts the developmental trajectory of progenitor cells, and leads to the differentiation of supernumerary EE.

IMD Pathway Activity Promotes the Development of Notch-Mediated Intestinal Tumors.

As bacterial challenges enhance *Notch*-deficient tumor formation (Apidianakis et al., 2009), and ImdCA influences *Notch*-dependent events, we asked what effects persistent immune signals have on models of *Notch*-deficient tumorigenesis in the posterior midgut. To answer this question, we used a validated, inducible RNAi line that blocks *Notch* signaling in adult progenitors ($esg^{ts}>N^{RNAi}$). As anticipated, the posterior midguts of $esg^{ts}>N^{RNAi}$ flies contain clusters of small, Prospero positive tumors (Figure 7 I, arrowhead) flanked by fields of regular intestinal tissue (Figure 7 J, area marked in red). The ability of $esg^{ts}>N^{RNAi}$ to promote tumorigenesis appears to require extrinsic inputs from the microbiome, as removal of the gut microbiome prevented the appearance of Prospero positive clusters in $esg^{ts}>N^{RNAi}$ posterior midguts (Figure 7 L-N). This observation matches an earlier report that growth of *Notch* loss-of-function tumors requires stress-induced mitogenic cues (Patel et al., 2015).

Whereas elimination of the microbiome blocked tumorigenesis in $esg^{ts}>N^{RNAi}$ flies, co-expression of ImdCA with N^{RNAi} ($esg^{ts}>N^{RNAi}$; *CA*) exacerbated the formation of midgut tumors. We invariably detected large patches of Prospero positive cells in $esg^{ts}>N^{RNAi}$; *CA* posterior midguts, with very few large cells characteristic of mature EC (Figure 7 O-Q). The size and disorganized arrangement of tumors in $esg^{ts}>N^{RNAi}$; *CA* flies prevented us from accurately quantifying tumor numbers per gut, but the phenotype was consistent across all midguts examined (n = 5). To determine if ImdCA alone provides sufficient stress signals to promote tumorigenesis in this *Notch* loss-of-function model, we examined the posterior midguts of germ-free $esg^{ts}>N^{RNAi}$; *CA* flies. We found that all midguts of germ-free $esg^{ts}>CA, N^{RNAi}$ flies had large patches of Prospero positive tumors, very few large polyploid ECs, and an accumulation of small

cells (Figure 7 R-T). This phenotype is remarkably similar to one described earlier for bacterial infection of *esg*^{ts}>*N*^{RNAi} flies (Jiang et al., 2009), and shows that immune signaling in progenitor cells alone is sufficient to promote *Notch*-dependent tumor growth in adult midguts.

DISCUSSION

Animal genomes encode evolutionarily conserved systems that neutralize potentially harmful microbes. For example, the innate immune response rapidly activates antibacterial defenses upon detection of microbe-associated molecular patterns. Most immune systems are subject to dueling regulatory requirements in the host. Activation of innate defenses is important for control of the intestinal microbiota (Thaiss et al., 2016). However, chronic innate immune activity promotes inflammatory diseases and potentiates tumorigenesis in the gut (Grivennikov et al., 2010). In this study, we used the genetically accessible fruit fly to activate immune responses exclusively in intestinal progenitor cells. We showed that persistent immune activity causes intestinal hyperplasia, disrupts progenitor cell differentiation, and fuels Notch-dependent tumorigenesis. Our studies match reports of relationships between the microbiota, inflammation and colorectal cancer (Belkaid and Hand, 2014, Irrazabal et al., 2014), and uncover an unanticipated requirement for regulated innate immune activity in the overall maintenance of progenitor cell homeostasis in the fly.

In *Drosophila*, several homeostatic devices control progenitor cell proliferation and differentiation, often in response to bacterial products (Amcheslavsky et al., 2009, Buchon et al., 2009, Jiang et al., 2009). For example, flies raised in the absence of a microbiome undergo fewer mitoses in the midgut (Buchon et al., 2009). In addition, flies raised in a germ-free environment have atypical numbers of prospero-positive EE cells; a lower density of ECs; and show a deregulated expression of Notch pathway components (Broderick et al., 2014). It is unclear how much of this response requires an intact IMD pathway, although recent transcriptional work

established that mutations of the IMD pathway impact numerous aspects of intestinal transcription (Broderick et al., 2014, Erkosar et al., 2014), including Notch pathway components (Broderick et al., 2014). Our work shows that expression of ImdCA in progenitor cells alone recapitulates defining features of host responses to gut microbes. For example, of the 253 genes differentially expressed in the intestines of conventionally-reared flies compared to germ-free flies, 92 are affected by expression ImdCA. Additionally, expression of ImdCA in progenitor cells boosts intestinal mitoses, affects EE cell differentiation, and increases EC density. Combined, these data implicate the IMD pathway as a novel regulator of intestinal homeostasis.

As the microbiome induces progenitor cell proliferation, we initially assumed that ImdCA-dependent hyperplasia was the result of a dysbiosis in the gut caused by immune activity. However, expression of ImdCA does not influence microbiome composition, suggesting that the *Drosophila* microbiome effectively counters innate immune defenses. This matches experimental data that commensal bacteria effectively overcome host innate defenses in several models. For example, many gut-resident *Firmicutes* and *Bacteroidetes* are not susceptible to antimicrobial peptides (Cullen et al., 2015), and NOD deficient mice do not display dysbiosis (Robertson et al., 2013, Shanahan et al., 2014). These observations lead us propose that constitutive activation of IMD acts directly on the host to induces intestinal hyperplasia. Our model is supported by the observation that ImdCA effectively promotes *Notch* loss-of-function tumor growth in conventionally-reared and germ-free animals. We believe that the ability of ImdCA to promote Notch-dependent tumors is of particular significance in the context of aging. As flies age, clones of *Notch* mutant cells spontaneously develop in the intestine (Siudeja et al., 2015), and host immune activity gradually rises (Buchon et al., 2009). Our data suggest that age-dependent

increases in immune activity may contribute to the formation, or growth, of Notch-dependent tumors in the fly. Indeed, we found that elimination of the microbiome was sufficient to arrest the appearance of Notch-dependent tumors.

The role of Notch in tumorigenesis is not restricted to flies. Several studies established clear links between deregulated Notch activity and carcinogenesis in vertebrates (Rizzo et al., 2008, Shih Ie and Wang, 2007). Colorectal cancer lines and adenocarcinomas express elevated levels of Notch1 and Notch 2 (Fre et al., 2009, Guilmeau et al., 2010, Reedijk et al., 2008, Sikandar et al., 2010). In addition, manipulations of Notch pathway activity modify tumorigenesis in mouse models of colorectal cancer (Fre et al., 2009, Rodilla et al., 2009). The mechanisms that activate Notch in colon cancer are unclear at present. Given the broad conservation of immune activity and Notch signaling in the guts of flies and mammals, our work raises the possibility that chronic inflammation is a long-term activator of Notch-dependent tumorigenesis. The data this study present a simple model to precisely describe the relationships between intestinal immune activity and the formation of Notch-dependent tumors.

EXPERIMENTAL PROCEDURES

Drosophila husbandry.

All flies were raised on standard corn meal medium (Nutri-Fly Bloomington Formulation, Genesse Scientific). To generate germ-free animals, we raised freshly eclosed adult flies on sterile food containing an antibiotic cocktail (100 µg/ml Ampicillin, 100 µg/ml Neomycin, 100 µg/ml Metronidazole and 50 µg/ml Vancomycin). This protocol allowed us to raise larvae in the presence of a conventional microbiome, and restrict our examination of germ-free phenotypes to the adult life stage. For 16S deep-sequencing, we raised freshly eclosed virgin females flies on antibiotic medium for 5 d at 18°C, then switched to sterile antibiotic-free food for 1 d. Next, flies were fed a homogenate prepared from w^{1118} flies for 16 h. Afterwards, flies were raised on sterile antibiotic-free food at 18°C for 7 d. Flies were moved to 29°C for another 7 days, and 10 guts/sample were dissected. We extracted microbial DNA with the UltraClean® Microbial DNA Isolation Kit (MoBio Laboratories Inc.), and amplified 16S DNA with Platinum® PFX Taq (Invitrogen), followed by purification with the QIAquick® PCR Purification Kit (Qiagen). Concentration was measured on the Qubit® 2.0 (Invitrogen) and 1 ng was used for library prep. Libraries were prepared using the Nextera XT DNA Library Preparation Kit (Illumina). We purified libraries using Ampure Beads (Qiagen) and quantified using the Qubit® 2.0 (Invitrogen) and Bioanalyzer 2100 (Agilent). Pooled libraries were loaded on the Miseq (illumina) using the MiSeq Reagent Kit v3 (600-cycle) for sequencing. 16S sequences were assembled using DNASTAR Navigator, and annotated with the greengenes database. For infection studies, freshly eclosed flies were raised for 5 d at 18°C, then switched to 29°C for 2 d. 24 h before infection 100 µl of a

V. cholerae C6706 glycerol stock was spread on LB agar plates and grown at 29°C. Flies were starved for 2 h before infection. The bacterial lawn was scraped from the plate and mixed into LB broth, then diluted to an OD600 of 0.125, flies were fed 3ml of the bacterial on a cotton plug, and dead flies counted every 2-4 h. To generate mitotic clones, flies were raised at 18°C for 5-6 d, incubated at 37°C for 2 h, and raised for an additional 8-10 days at 25°C.

Cell culture and molecular biology.

The Imd expression construct used in this study has been described elsewhere (Guntermann and Foley, 2011). To generate ImdCA, we cloned truncated Imd with into the pENTR/D-TOPO plasmid (Invitrogen). We recombined TOPO-ImdCA with pAWM, or pTW (LR recombination, Invitrogen) to generate ImdCA-6myc and UAS-ImdCA expression plasmids. Immunoprecipitation and Western blot protocols have been described in detail elsewhere (Guntermann and Foley, 2011). For immunoprecipitation assays, we incubated cell lysate with mouse anti-HA (Sigma, 1:500) at 4°C overnight, added protein G-Sepharose beads and incubated for an additional hour at 4°C. Beads were pelleted by centrifugation at 300 X g for 30 s and washed in lysis buffer three times. After discarding the supernatant, beads were re-suspended in 2X sample buffer, and analyzed by Western blot.

Gene expression analysis.

We used TRIZOL to prepare RNA from dissected adult intestines using an established protocol (Guntermann and Foley, 2011). Microarray studies were performed in triplicate on virgin flies that we raised on regular or antibiotic-treated food food for 10-11 days at 29°C. We then shifted

flies to 29°C for another 2 days, after which guts were dissected for RNA extraction (5 females and 5 males per sample). We used 100 ng purified RNA to make labeled cRNA for microarrays using the GeneChip® 3' IVT Plus Reagent Kit (Affymetrix), then fragmented cRNA and then hybridized to the GeneChip®Drosophila Genome 2.0 Array (Affymetrix). Preliminary analysis was done in the Transciptome Analysis Console (TAC) software (Affymetrix). We analyzed gene expression data using FlyMINE (Lyne et al., 2007) and Panther (Thomas et al., 2003). Array data has been submitted to the NCBI GEO database (accession ID: GSE89445). For qPCR studies, we prepared 1 µg cDNA from purified RNA using qScript cDNA Supermix (Quanta Biosciences, Inc.) and then performed qPCR using the PerfeCTa® SYBR®Green FastMix (Quanta Biosciences, Inc.). All qPCR studies were performed in triplicate. In each case, expression levels were normalized to *actin*.

Immunofluorescence.

The immunofluorescence protocol used in this study has been described in detail elsewhere (Petkau et al., 2014). All immunofluorescence images were prepared from the posterior midgut of adult flies at a distance of approximately 50 µM from the hindgut transition. To quantify phospho-histone H3 positive cells, guts were visualized under the microscope and scanned from posterior midgut (hindgut transition area) to anterior midgut (crop). To quantify Prospero positive cells, we used the Columbus software to identify which Hoechst positive cells were also prospero positive. 3-D reconstructions were created with Volocity® 6.3 (Perkin Elmer).

AUTHOR CONTRIBUTIONS

K.P., S.G., and E.F. conceived and designed experiments; K.P., and S.G. performed the experiments; K.P. and E.F performed data analysis and wrote the paper.

ACKNOWLEDGEMENTS

Transgenic flies were provided by Bruce Edgar (*esg*^{ts}), Bruno Lemaitre (*dredd*), the Bloomington *Drosophila* stock Center (*cgGAL4* ; *GAL80*^{ts}), and the Vienna *Drosophila* Resource Center (*N*^{RNAi}). The research was funded by a grant from the Canadian Institutes of Health Research to EF (MOP 77746). We acknowledge the microscopy support from Dr. Stephen Ogg and the Faculty of Medicine and Dentistry core imaging service, the Cell Imaging Centre, University of Alberta.

REFERENCES

AMCHESLAVSKY, A., JIANG, J. & IP, Y. T. 2009. Tissue damage-induced intestinal stem cell division in Drosophila. *Cell Stem Cell,* 4**,** 49-61.

APIDIANAKIS, Y., PITSOULI, C., PERRIMON, N. & RAHME, L. 2009. Synergy between bacterial infection and genetic predisposition in intestinal dysplasia. *Proc Natl Acad Sci U S A,* 106**,** 20883-8.

BELKAID, Y. & HAND, T. W. 2014. Role of the microbiota in immunity and inflammation. *Cell,* 157**,** 121-41.

BITEAU, B. & JASPER, H. 2011. EGF signaling regulates the proliferation of intestinal stem cells in Drosophila. *Development,* 138**,** 1045-55.

BRODERICK, N. A., BUCHON, N. & LEMAITRE, B. 2014. Microbiota-induced changes in drosophila melanogaster host gene expression and gut morphology. *MBio,* 5**,** e01117-14.

BUCHON, N., BRODERICK, N. A., CHAKRABARTI, S. & LEMAITRE, B. 2009. Invasive and indigenous microbiota impact intestinal stem cell activity through multiple pathways in Drosophila. *Genes Dev,* 23**,** 2333-44.

BUCHON, N., BRODERICK, N. A. & LEMAITRE, B. 2013. Gut homeostasis in a microbial world: insights from Drosophila melanogaster. *Nat Rev Microbiol,* 11**,** 615-26.

BUCHON, N., SILVERMAN, N. & CHERRY, S. 2014. Immunity in Drosophila melanogaster--from microbial recognition to whole-organism physiology. *Nat Rev Immunol,* 14**,** 796-810.

CHO, I. & BLASER, M. J. 2012. The human microbiome: at the interface of health and disease. *Nat Rev Genet,* 13**,** 260-70.

CROSNIER, C., VARGESSON, N., GSCHMEISSNER, S., ARIZA-MCNAUGHTON, L., MORRISON, A. & LEWIS, J. 2005. Delta-Notch signalling controls commitment to a secretory fate in the zebrafish intestine. *Development,* 132**,** 1093-104.

CULLEN, T. W., SCHOFIELD, W. B., BARRY, N. A., PUTNAM, E. E., RUNDELL, E. A., TRENT, M. S., DEGNAN, P. H., BOOTH, C. J., YU, H. & GOODMAN, A. L. 2015. Gut microbiota. Antimicrobial peptide resistance mediates resilience of prominent gut commensals during inflammation. *Science,* 347**,** 170-5.

DUSHAY, M. S., ASLING, B. & HULTMARK, D. 1996. Origins of immunity: Relish, a compound Rel-like gene in the antibacterial defense of Drosophila. *Proc Natl Acad Sci U S A,* 93**,** 10343-7.

ERKOSAR, B., DEFAYE, A., BOZONNET, N., PUTHIER, D., ROYET, J. & LEULIER, F. 2014. Drosophila microbiota modulates host metabolic gene expression via IMD/NF-kappaB signaling. *PLoS One,* 9**,** e94729.

FRE, S., HUYGHE, M., MOURIKIS, P., ROBINE, S., LOUVARD, D. & ARTAVANIS-TSAKONAS, S. 2005. Notch signals control the fate of immature progenitor cells in the intestine. *Nature,* 435**,** 964-8.

FRE, S., PALLAVI, S. K., HUYGHE, M., LAE, M., JANSSEN, K. P., ROBINE, S., ARTAVANIS-TSAKONAS, S. & LOUVARD, D. 2009. Notch and Wnt signals cooperatively control cell proliferation and tumorigenesis in the intestine. *Proc Natl Acad Sci U S A,* 106**,** 6309-14.

GRIVENNIKOV, S. I., GRETEN, F. R. & KARIN, M. 2010. Immunity, inflammation, and cancer. *Cell,* 140**,** 883-99.

GUILMEAU, S., FLANDEZ, M., MARIADASON, J. M. & AUGENLICHT, L. H. 2010. Heterogeneity of Jagged1 expression in human and mouse intestinal tumors: implications for targeting Notch signaling. *Oncogene,* 29**,** 992-1002.

GUNTERMANN, S. & FOLEY, E. 2011. The protein Dredd is an essential component of the c-Jun N-terminal kinase pathway in the Drosophila immune response. *J Biol Chem,* 286**,** 30284-94.

GUO, Z. & OHLSTEIN, B. 2015. Stem cell regulation. Bidirectional Notch signaling regulates Drosophila intestinal stem cell multipotency. *Science,* 350.

HONDA, K. & LITTMAN, D. R. 2016. The microbiota in adaptive immune homeostasis and disease. *Nature,* 535**,** 75-84.

HOOPER, L. V., LITTMAN, D. R. & MACPHERSON, A. J. 2012. Interactions between the microbiota and the immune system. *Science,* 336**,** 1268-73.

IRRAZABAL, T., BELCHEVA, A., GIRARDIN, S. E., MARTIN, A. & PHILPOTT, D. J. 2014. The multifaceted role of the intestinal microbiota in colon cancer. *Mol Cell,* 54**,** 309-20.

JIANG, H. & EDGAR, B. A. 2012. Intestinal stem cell function in Drosophila and mice. *Curr Opin Genet Dev,* 22**,** 354-60.

JIANG, H., PATEL, P. H., KOHLMAIER, A., GRENLEY, M. O., MCEWEN, D. G. & EDGAR, B. A. 2009. Cytokine/Jak/Stat signaling mediates regeneration and homeostasis in the Drosophila midgut. *Cell,* 137**,** 1343-55.

KAZANJIAN, A. & SHROYER, N. F. 2011. NOTCH Signaling and ATOH1 in Colorectal Cancers. *Curr Colorectal Cancer Rep,* 7**,** 121-127.

LEMAITRE, B. & MIGUEL-ALIAGA, I. 2013. The digestive tract of Drosophila melanogaster. *Annu Rev Genet,* 47**,** 377-404.

LHOCINE, N., RIBEIRO, P. S., BUCHON, N., WEPF, A., WILSON, R., TENEV, T., LEMAITRE, B., GSTAIGER, M., MEIER, P. & LEULIER, F. 2008. PIMS modulates immune tolerance by negatively regulating Drosophila innate immune signaling. *Cell Host Microbe,* 4**,** 147-58.

LYNE, R., SMITH, R., RUTHERFORD, K., WAKELING, M., VARLEY, A., GUILLIER, F., JANSSENS, H., JI, W., MCLAREN, P., NORTH, P., RANA, D., RILEY, T., SULLIVAN, J., WATKINS, X., WOODBRIDGE, M., LILLEY, K., RUSSELL, S., ASHBURNER, M., MIZUGUCHI, K. & MICKLEM, G. 2007. FlyMine: an integrated database for Drosophila and Anopheles genomics. *Genome Biol,* 8**,** R129.

MARIANES, A. & SPRADLING, A. C. 2013. Physiological and stem cell compartmentalization within the Drosophila midgut. *Elife,* 2**,** e00886.

MICCHELLI, C. A. & PERRIMON, N. 2006. Evidence that stem cells reside in the adult Drosophila midgut epithelium. *Nature,* 439**,** 475-9.

OHLSTEIN, B. & SPRADLING, A. 2006. The adult Drosophila posterior midgut is maintained by pluripotent stem cells. *Nature,* 439**,** 470-4.

OHLSTEIN, B. & SPRADLING, A. 2007. Multipotent Drosophila intestinal stem cells specify daughter cell fates by differential notch signaling. *Science,* 315**,** 988-92.

PAQUETTE, N., BROEMER, M., AGGARWAL, K., CHEN, L., HUSSON, M., ERTURK-HASDEMIR, D., REICHHART, J. M., MEIER, P. & SILVERMAN, N. 2010. Caspase-mediated cleavage, IAP binding, and ubiquitination: linking three mechanisms crucial for Drosophila NF-kappaB signaling. *Mol Cell,* 37**,** 172-82.

PATEL, P. H., DUTTA, D. & EDGAR, B. A. 2015. Niche appropriation by Drosophila intestinal stem cell tumours. *Nat Cell Biol,* 17**,** 1182-92.

PATEL, P. H. & EDGAR, B. A. 2014. Tissue design: how Drosophila tumors remodel their neighborhood. *Semin Cell Dev Biol,* 28**,** 86-95.

PEIGNON, G., DURAND, A., CACHEUX, W., AYRAULT, O., TERRIS, B., LAURENT-PUIG, P., SHROYER, N. F., VAN SEUNINGEN, I., HONJO, T., PERRET, C. & ROMAGNOLO, B. 2011. Complex interplay between beta-catenin signalling and Notch effectors in intestinal tumorigenesis. *Gut,* 60**,** 166-76.

PERDIGOTO, C. N., SCHWEISGUTH, F. & BARDIN, A. J. 2011. Distinct levels of Notch activity for commitment and terminal differentiation of stem cells in the adult fly intestine. *Development,* 138**,** 4585-95.

PETKAU, K., PARSONS, B. D., DUGGAL, A. & FOLEY, E. 2014. A deregulated intestinal cell cycle program disrupts tissue homeostasis without affecting longevity in Drosophila. *J Biol Chem,* 289**,** 28719-29.

REEDIJK, M., ODORCIC, S., ZHANG, H., CHETTY, R., TENNERT, C., DICKSON, B. C., LOCKWOOD, G., GALLINGER, S. & EGAN, S. E. 2008. Activation of Notch signaling in human colon adenocarcinoma. *Int J Oncol,* 33**,** 1223-9.

RIZZO, P., OSIPO, C., FOREMAN, K., GOLDE, T., OSBORNE, B. & MIELE, L. 2008. Rational targeting of Notch signaling in cancer. *Oncogene,* 27**,** 5124-31.

ROBERTSON, S. J., ZHOU, J. Y., GEDDES, K., RUBINO, S. J., CHO, J. H., GIRARDIN, S. E. & PHILPOTT, D. J. 2013. Nod1 and Nod2 signaling does not alter the composition of intestinal bacterial communities at homeostasis. *Gut Microbes,* 4**,** 222-31.

RODILLA, V., VILLANUEVA, A., OBRADOR-HEVIA, A., ROBERT-MORENO, A., FERNANDEZ-MAJADA, V., GRILLI, A., LOPEZ-BIGAS, N., BELLORA, N., ALBA, M. M., TORRES, F., DUNACH, M.,

SANJUAN, X., GONZALEZ, S., GRIDLEY, T., CAPELLA, G., BIGAS, A. & ESPINOSA, L. 2009. Jagged1 is the pathological link between Wnt and Notch pathways in colorectal cancer. *Proc Natl Acad Sci U S A,* 106**,** 6315-20.

SHANAHAN, M. T., CARROLL, I. M., GROSSNIKLAUS, E., WHITE, A., VON FURSTENBERG, R. J., BARNER, R., FODOR, A. A., HENNING, S. J., SARTOR, R. B. & GULATI, A. S. 2014. Mouse Paneth cell antimicrobial function is independent of Nod2. *Gut,* 63**,** 903-10.

SHIH IE, M. & WANG, T. L. 2007. Notch signaling, gamma-secretase inhibitors, and cancer therapy. *Cancer Res,* 67**,** 1879-82.

SIKANDAR, S. S., PATE, K. T., ANDERSON, S., DIZON, D., EDWARDS, R. A., WATERMAN, M. L. & LIPKIN, S. M. 2010. NOTCH signaling is required for formation and self-renewal of tumor-initiating cells and for repression of secretory cell differentiation in colon cancer. *Cancer Res,* 70**,** 1469-78.

SIUDEJA, K., NASSARI, S., GERVAIS, L., SKORSKI, P., LAMEIRAS, S., STOLFA, D., ZANDE, M., BERNARD, V., RIO FRIO, T. & BARDIN, A. J. 2015. Frequent Somatic Mutation in Adult Intestinal Stem Cells Drives Neoplasia and Genetic Mosaicism during Aging. *Cell Stem Cell,* 17**,** 663-74.

STANGER, B. Z., DATAR, R., MURTAUGH, L. C. & MELTON, D. A. 2005. Direct regulation of intestinal fate by Notch. *Proc Natl Acad Sci U S A,* 102**,** 12443-8.

TAKASHIMA, S., ADAMS, K. L., ORTIZ, P. A., YING, C. T., MORIDZADEH, R., YOUNOSSI-HARTENSTEIN, A. & HARTENSTEIN, V. 2011. Development of the Drosophila entero-endocrine lineage and its specification by the Notch signaling pathway. *Dev Biol,* 353**,** 161-72.

THAISS, C. A., ZMORA, N., LEVY, M. & ELINAV, E. 2016. The microbiome and innate immunity. *Nature,* 535**,** 65-74.

THOMAS, P. D., CAMPBELL, M. J., KEJARIWAL, A., MI, H., KARLAK, B., DAVERMAN, R., DIEMER, K., MURUGANUJAN, A. & NARECHANIA, A. 2003. PANTHER: a library of protein families and subfamilies indexed by function. *Genome Res,* 13**,** 2129-41.

VAN ES, J. H., VAN GIJN, M. E., RICCIO, O., VAN DEN BORN, M., VOOIJS, M., BEGTHEL, H., COZIJNSEN, M., ROBINE, S., WINTON, D. J., RADTKE, F. & CLEVERS, H. 2005. Notch/gamma-secretase inhibition turns proliferative cells in intestinal crypts and adenomas into goblet cells. *Nature,* 435**,** 959-63.

WLODARSKA, M., KOSTIC, A. D. & XAVIER, R. J. 2015. An integrative view of microbiome-host interactions in inflammatory bowel diseases. *Cell Host Microbe,* 17**,** 577-91.

FIGURE LEGENDS

Figure 1. A truncated Imd protein activates innate immune responses. (A) Schematic representation of C-terminally myc-tagged Imd and ImdCA. Iap Binding Motif (IBM) and death domain (DD) are indicated. Western blots show lysates of untransfected S2 cells (lane 1) S2 cells transfected with expression constructs for Imd-6myc (lane 2), and ImdCA-6myc (lane 3). Numbers indicated molecular weights in kDa, and the membrane was probed with Tubulin as a loading control. **(B)** S2 cells were transfected with the indicated expression constructs and input samples (blots labeled INPUT) were probed for the indicated antigens. Anti-HA immunoprecipitates (blots labeled IP:HA) were probed with the indicated antibodies. **(C-E)** Quantification of the relative expression levels of *dpt* and *att* in flies raised at 29°C for the indicated time. Survival curves of *esg*^{ts}*>CA* and *esg*^{ts} flies raised at 29°C for two days, and then challenged with *Vibrio cholerae*.

Figure 2. ImdCA and the microbiome interact to control gut transcription. A-B: Graphic representation of biological functions dysregulated in *esg*^{ts}*>CA* flies relative to *esg*^{ts} flies raised under conventional (A) or germ-free conditions (B). **C-D:** Graphic representation of biological functions dysregulated in conventional flies relative to germ-free flies in the absence (C) or presence (D) of ImdCA expression. For A-D, numbers indicated total numbers of dysregulated genes. Genes with unknown function were not included in pie charts. **(E-F)** Heatmap of significance scores for gene ontology terms (minimum 5 genes in each term) that were significantly dysregulated in *esg*^{ts}*>CA* flies relative to *esg*^{ts} flies (E), or conventionally-reared relative to germ-free flies (F). In E, GO terms are further subdivided into terms that were

dysregulated in conventionally-reared or germ-free flies. In F, GO terms are subdivided into terms that were dysregulated in *esg*^{ts} flies and *esg*^{ts}*>CA* flies.

Figure 3: A-D: Relative expression of totM (A), pirk (B), pgrp-sc1 (C) and cec (D) in the dissected intestines of conventionally-reared or germ-free *esg*^{ts} flies or *esg*^{ts}*>CA* flies. For each assay, expression levels were reported relative to those observed in germ-free *esg*^{ts} flies. Comparisons were performed with a Sidak's multiple comparison test. Values show the Sidak's t value for the respective tests. **E:** Number of genes and GO terms that were up or downregulated in *esg*^{ts}*>CA* flies relative to *esg*^{ts} flies raised under conventional (CR) or germ-free (GF) conditions. **G:** Number of genes and GO terms that were up or downregulated in conventionally-reared flies relative to germ-free flies of the indicated genotypes.

Figure 4. Induced expression of ImdCA in intestinal progenitor cells does not have a substantial impact on gut microbiome composition. Heat map analysis of microbial original taxonomic unit representation in dissected midguts of the indicated genotypes. All flies were raised under identical conditions, and fed the same homogenate at the same time.

Figure 5: A-B Homeostatic regulators (A) and Notch pathway components (B) that were dysregulated in *esg*^{ts}*>CA* flies relative to *esg*^{ts} flies. **B-E:** Visualization of mitotic clones in wild type flies. Arrowheads indicate three large enterocytes. **F-I:** Visualization of mitotic clones that express *imdCA*. All images were taken at 60X magnification and scale bars show 15 µm **J:** Percentage of

large, enterocyte-type cells in wild type clones and *imdCA* positive clones. Comparisons were performed with a student's t test.

Figure 6. Intestinal hyperplasia in the posterior midguts of *esg^{ts}>CA* flies. Immunofluorescence imaging of the posterior midguts of *esg^{ts}>CA* and *esg^{ts}* flies raised at 29°C for two or 26 days as indicated. Each midgut was stained with Armadillo (to indicate cell borders), and Prospero to reveal enteroendocrine cells **(A, E, I, M)**; Hoechst to reveal nuclei **(B, F, J and N)**; and GFP was visualized to reveal progenitor cells **(C, G, K, Q)**. The respective panels were false colored and merged in D, H, L and P. All images were taken at 40X magnification and scale bars show 25 µm. **(Q-S)** Three dimensional reconstructions of sections of the posterior midguts of the indicated genotypes. **(T)** Number of mitotic cells in the intestines of *esg^{ts}>CA* and *esg^{ts}* flies raised at 29°C for 14 and 24 days.

Figure 7. ImdCA promotes tumorigenesis in Notch-deficient progenitor cells. (A-F) Midguts of *esg^{ts}* and *esg^{ts}>CA* flies were stained for DNA (A, D), and Prospero (B, E). Images were false-colored and merged in C and F, with DNA in blue, and Prospero in red. All images were taken at 40X magnification and scale bars show 25 µm. **G:** Automated quantification of total nuclei in a given field for flies of both genotypes. **H:** Total percentage of Prospero positive cells in the same fields. For G and H comparisons were performed with a student's t test. **N-T:** Visualization of tumorigenesis in *esg^{ts}>N^{RNAi}* and *esg^{ts}>N^{RNAi}; CA* flies. Posterior midguts were stained for Prospero (I, L, O, R) and DNA (L, M, P, S) in conventionally-reared *esg^{ts}>N^{RNAi}*; flies (I-K); germ-free *esg^{ts}>N^{RNAi}* flies (L-N); conventionally-reared *esg^{ts}>N^{RNAi}; CA* flies (O-Q); and germ-free *esg^{ts}>N^{RNAi}*;

CA flies (R-T). Clusters of Prospero-positive cells are indivated with arrowheads. All images were taken at 20X magnification and scale bars show 50 µm A field of regularly organized epithelium in $esg^{ts}>N^{RNAi}$ flies is showed with a red line. Panels K, N, Q, and T show three dimensional reconstructions of Z-sections prepared from the respective genotypes.

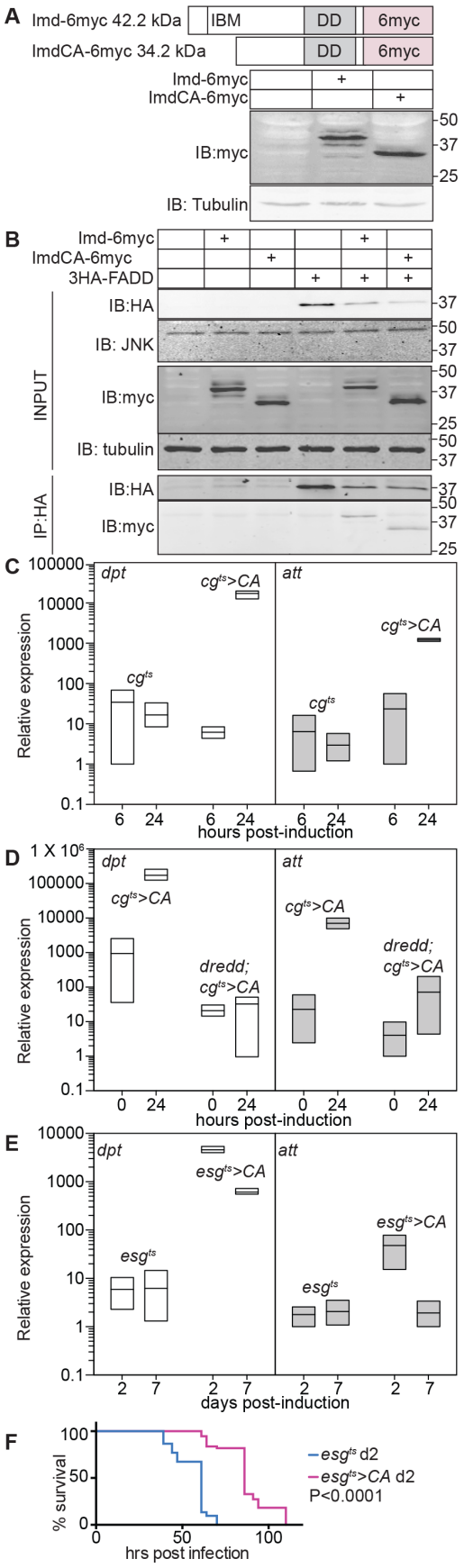
A
Imd-6myc 42.2 kDa
IBM
DD
6myc
ImdCA-6myc 34.2 kDa
Imd-6myc
ImdCA-6myc
IB:myc
IB: Tubulin
B
3HA-FADD
INPUT
IP:HA
IB:HA
IB: JNK
IB: tubulin
C
dpt
att
Relative expression
hours post-induction
D
E
esg^ts>CA
esg^ts
days post-induction
F
% survival
hrs post infection
esg^ts d2
esg^ts>CA d2
P<0.0001

FIGURE 1

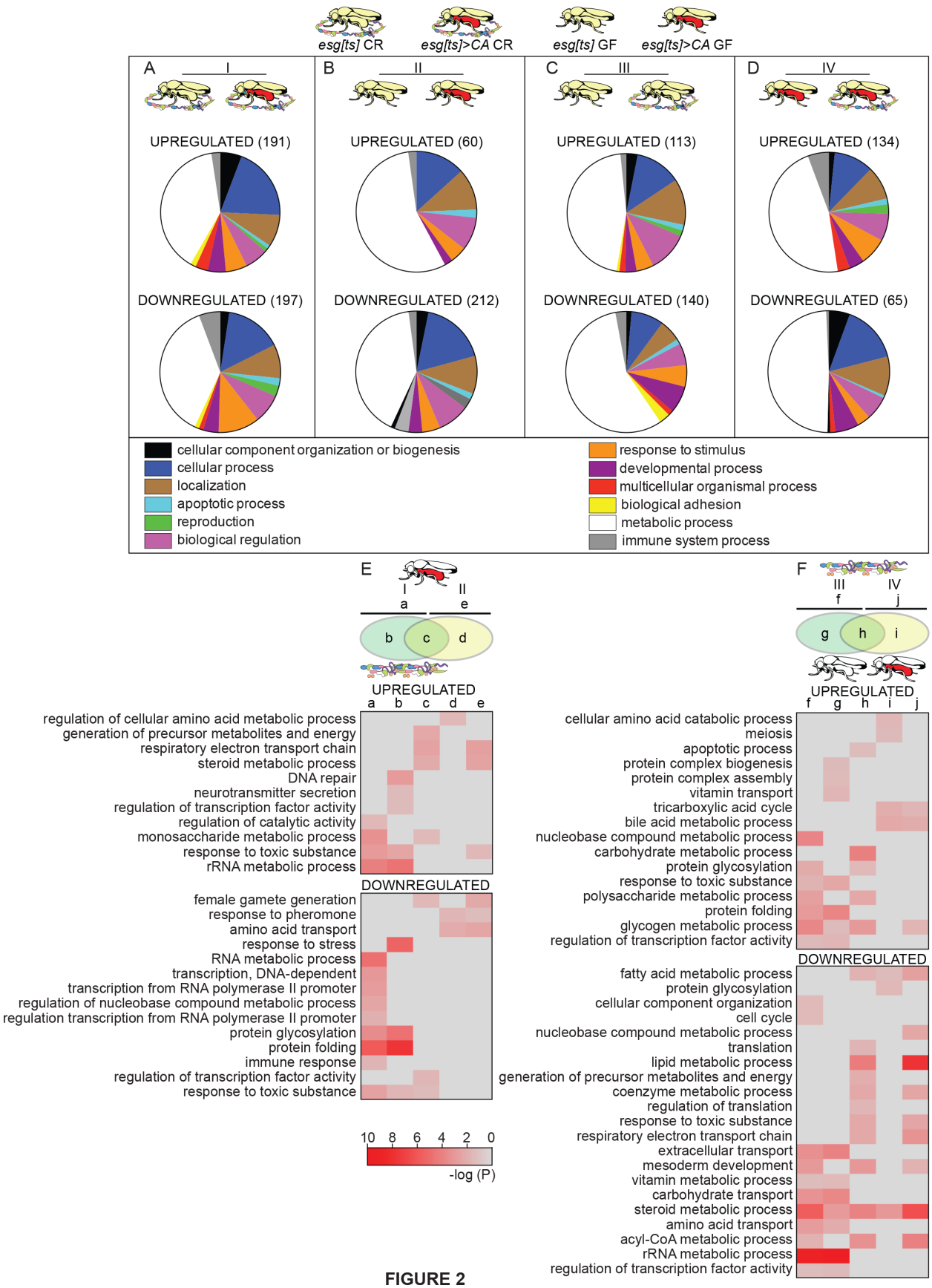
esg[ts] CR
esg[ts]>CA CR
esg[ts] GF
esg[ts]>CA GF
A
I
UPREGULATED (191)
DOWNREGULATED (197)
B
II
UPREGULATED (60)
DOWNREGULATED (212)
C
III
UPREGULATED (113)
DOWNREGULATED (140)
D
IV
UPREGULATED (134)
DOWNREGULATED (65)
cellular component organization or biogenesis
cellular process
localization
apoptotic process
reproduction
biological regulation
response to stimulus
developmental process
multicellular organismal process
biological adhesion
metabolic process
immune system process
E
I
II
a
e
b
c
d
UPREGULATED
a b c d e
regulation of cellular amino acid metabolic process
generation of precursor metabolites and energy
respiratory electron transport chain
steroid metabolic process
DNA repair
neurotransmitter secretion
regulation of transcription factor activity
regulation of catalytic activity
monosaccharide metabolic process
response to toxic substance
rRNA metabolic process
DOWNREGULATED
female gamete generation
response to pheromone
amino acid transport
response to stress
RNA metabolic process
transcription, DNA-dependent
transcription from RNA polymerase II promoter
regulation of nucleobase compound metabolic process
regulation transcription from RNA polymerase II promoter
protein glycosylation
protein folding
immune response
regulation of transcription factor activity
response to toxic substance
10 8 6 4 2 0
-log (P)
F
III
IV
f
j
g
h
i
UPREGULATED
f g h i j
cellular amino acid catabolic process
meiosis
apoptotic process
protein complex biogenesis
protein complex assembly
vitamin transport
tricarboxylic acid cycle
bile acid metabolic process
nucleobase compound metabolic process
carbohydrate metabolic process
protein glycosylation
response to toxic substance
polysaccharide metabolic process
protein folding
glycogen metabolic process
regulation of transcription factor activity
DOWNREGULATED
fatty acid metabolic process
protein glycosylation
cellular component organization
cell cycle
nucleobase compound metabolic process
translation
lipid metabolic process
generation of precursor metabolites and energy
coenzyme metabolic process
regulation of translation
response to toxic substance
respiratory electron transport chain
extracellular transport
mesoderm development
vitamin metabolic process
carbohydrate transport
steroid metabolic process
amino acid transport
acyl-CoA metabolic process
rRNA metabolic process
regulation of transcription factor activity

FIGURE 2

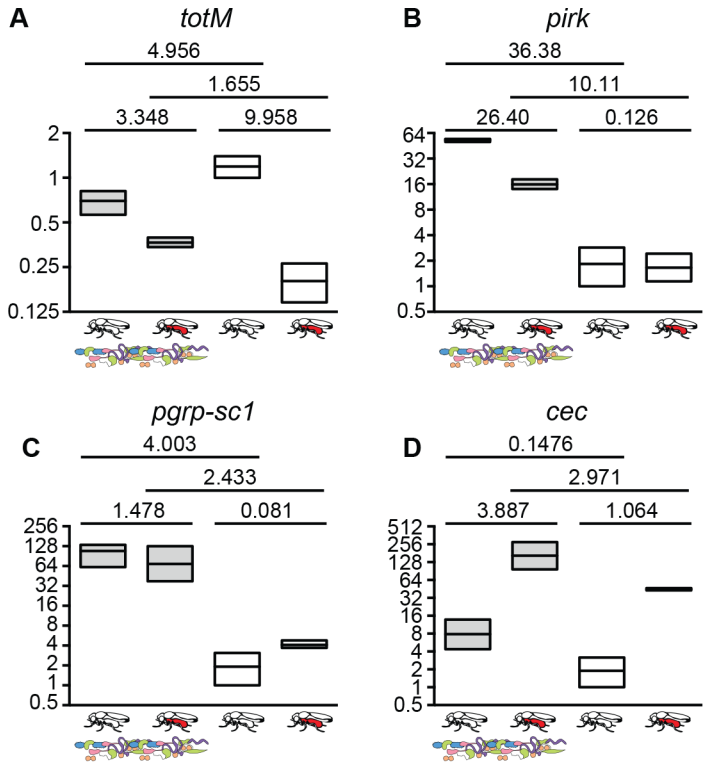

E

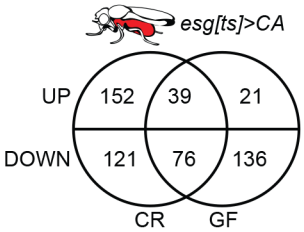

esg[ts]>CA response.	CR	GF
IMMUNE RESPONSE	16	11
SIGNAL TRANSDUCTION	38	12
MAINTENANCE OF STEM CELL IDENTITY	4	
DEVELOPMENT	9	
METABOLISM	63	31
TRANSPORT	21	19
OXIDATION-REDUCTION	17	11
ION HOMEOSTASIS	5	5
STRESS RESPONSE	26	10
OTHER	19	20
CHITIN BINDING		8
STEROL INTERACTING		6

F

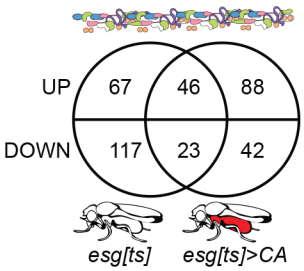

Microbiome response.	*esg[ts]*	*esg[ts] >CA*
IMMUNE RESPONSE	15	11
SIGNAL TRANSDUCTION	15	11
METABOLISM	58	40
TRANSPORT	23	11
OXIDATION-REDUCTION	11	11
ION HOMEOSTASIS		4
STRESS RESPONSE	16	5
OTHER	26	19
CHITIN BINDING	8	
STEROL INTERACTING		5

FIGURE 3

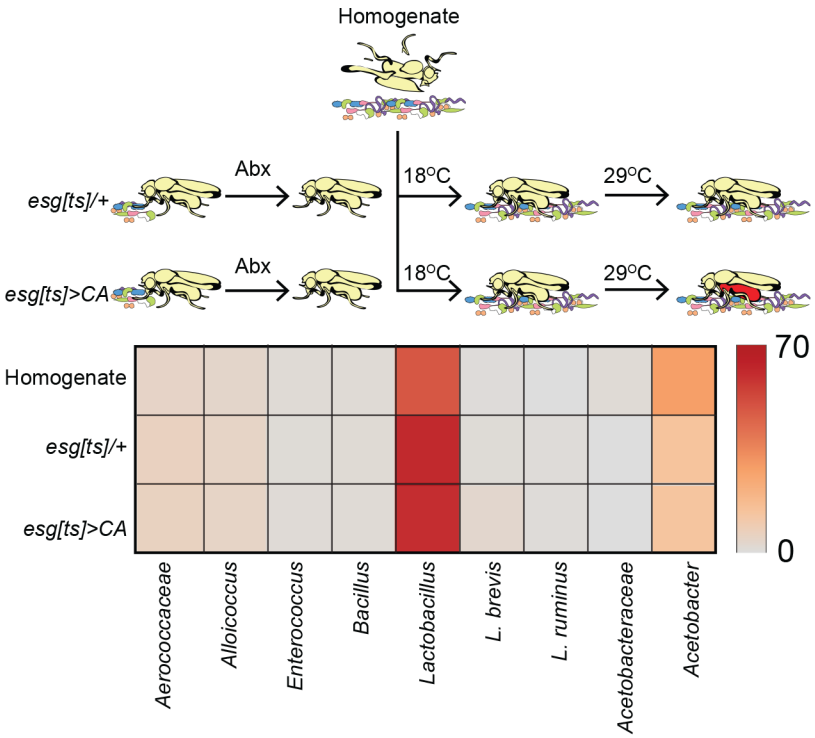
Homogenate
esg[ts]/+
Abx
18°C
29°C
esg[ts]>CA
Abx
18°C
29°C
Homogenate
esg[ts]/+
esg[ts]>CA
70
0
Aerococcaceae
Alloicoccus
Enterococcus
Bacillus
Lactobacillus
L. brevis
L. ruminus
Acetobacteraceae
Acetobacter

FIGURE 4

A

Gene	Function	Fold Change (*esgCA* V *esg*)	ANOVA p-value
MESK2	Ras signaling	-2.15	0.000349
gfzg	Ras signaling	-1.84	0.000116
cdi	Ras signaling	1.59	0.001404
Plzf	Ras signaling	-1.66	0.025787
CG42684	Ras signaling	2	0.000475
dock	Insulin signaling	-1.56	0.016287
srl	Insulin signaling	1.59	0.012109
sug	Insulin signaling	-1.68	0.025726
egr	JNK signaling	1.68	0.001723
Traf4	JNK signaling	1.64	0.000984
nmo	Wnt signaling	-1.98	0.000068
ebd1	Wnt signaling	1.53	0.008942
SOCS36E	JAK/STAT	-1.84	0.038907

B

Gene	Function	Fold Change (*esgCA* V *esg*)	ANOVA p-value
neur	Notch signaling	-1.55	0.001857
Nle	Notch signaling	1.63	0.010107
Rala	Notch signaling	2.07	0.000403
stv	Lateral Inhibition	-1.61	0.005874
Cam	Lateral Inhibition	-1.54	0.007552
CG13827	Lateral Inhibition	-1.74	0.003491
CG16713	Lateral Inhibition	-1.86	0.000181
CG5953	Lateral Inhibition	-1.81	0.002646
CG7631	Lateral Inhibition	-2.19	0.000129
CG9194	Lateral Inhibition	-1.89	0.001998

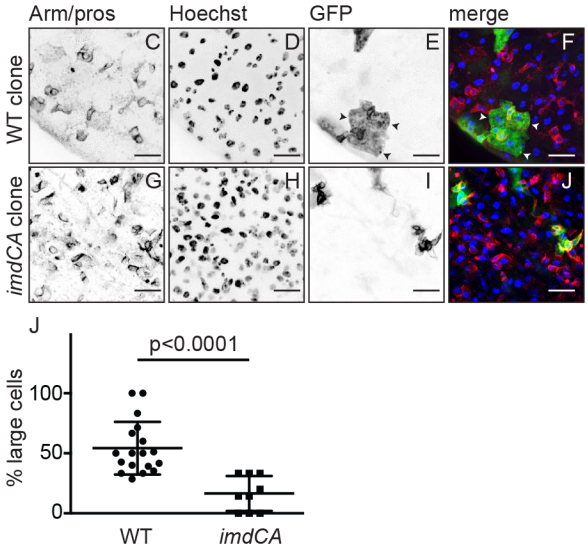

FIGURE 5

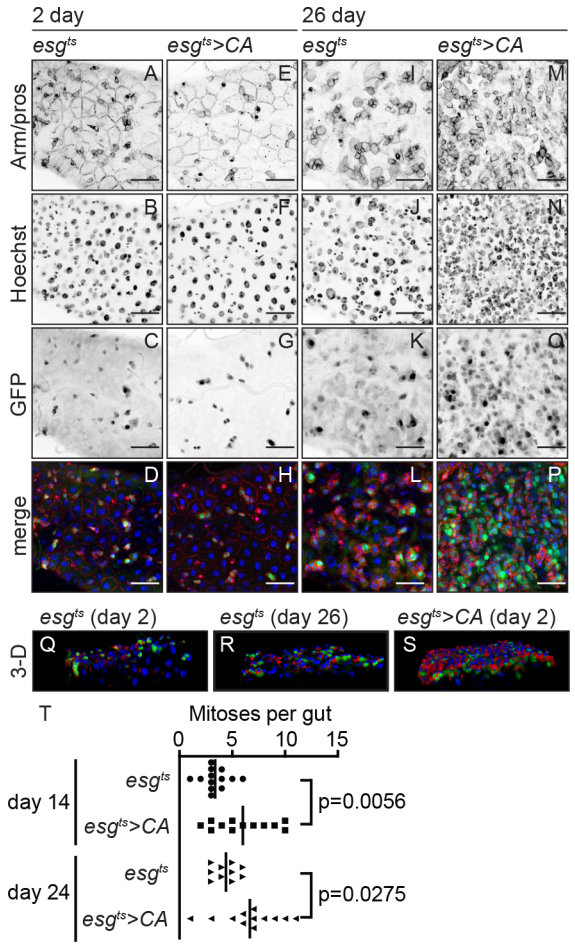
2 day
26 day
esgts
esgts>CA
esgts
esgts>CA
Arm/pros
Hoechst
GFP
merge
A
E
I
M
B
F
J
N
C
G
K
O
D
H
L
P
esgts (day 2)
esgts (day 26)
esgts>CA (day 2)
3-D
Q
R
S
T
Mitoses per gut
0
5
10
15
day 14
esgts
esgts>CA
p=0.0056
day 24
esgts
esgts>CA
p=0.0275

FIGURE 6

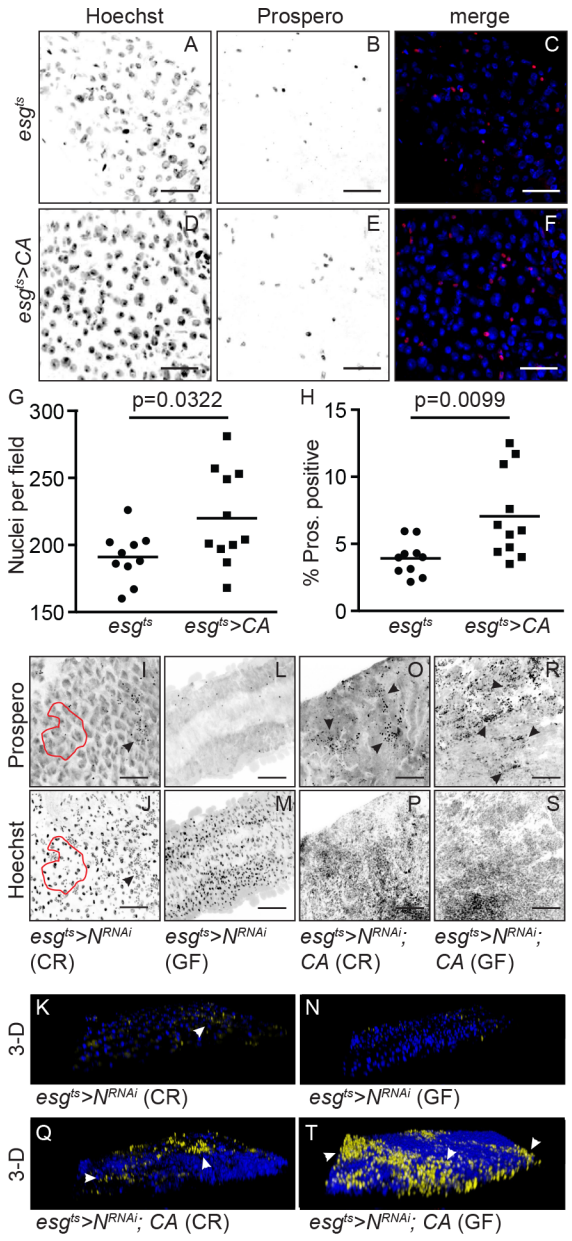
Hoechst
Prospero
merge
A
B
C
D
E
F
esg^ts
esg^ts>CA
G
p=0.0322
Nuclei per field
300
250
200
150
esg^ts
esg^ts>CA
H
p=0.0099
% Pros. positive
15
10
5
0
esg^ts
esg^ts>CA
Prospero
Hoechst
I
L
O
R
J
M
P
S
esg^ts>N^RNAi (CR)
esg^ts>N^RNAi (GF)
esg^ts>N^RNAi; CA (CR)
esg^ts>N^RNAi; CA (GF)
3-D
K
N
esg^ts>N^RNAi (CR)
esg^ts>N^RNAi (GF)
3-D
Q
T
esg^ts>N^RNAi; CA (CR)
esg^ts>N^RNAi; CA (GF)

FIGURE 7

SUPPLEMENTAL INFORMATION

Primers used in this study.

Gene	Forward Primer	Reverse Primer
pENTR/D-TOPO ImdCA	CACCGCAGCTCCCGTGGACGACAACG	CTAGCTGTTTGTCTTGCGC
16S	AGAGTTTGATCCTGGCTCAG	GGCTACCTTGTTACGACTT
att	AGTCACAACTGGCGGAAC	TGTTGAATAAATTGGCATGG
dpt	ACCGCAGTACCCACTCAATC	ACTTTCCAGCTCGGTTCTGA
actin	TGCCTCATCGCCGACATAA	CACGTCACCAGGGCGTAAT
totM	ACCGGAACATCGACAGCC	CCAGAATCCGCCTTGTGC
pirk	AGAGCACGAGCAGGGTAAATC	TGTTGTTCTCAATGCGGTACTC
pgrp-sc1	AAGCGATCGTCAACTATT	GAGAGCCACTTTGGAAACCA
cec	TGTAAGCTAGTTTATTTCTATGG	GATGAGCCTTTAATGTCC

Antibodies used in this study.

Antigen	Use	Source
Tubulin.	Western blot (1:1000)	Developmental Studies Hybridoma Bank E7
cMyc	Western blot (1:5000)	Sigma
HA	Western blot (1:4000)	Sigma

JNK	Western blot (1:4000)	Santa Cruz sc-571
Armadillo	Immunofluorescence (1:100)	Developmental Studies Hybridoma Bank N2 7A1
Prospero	Immunofluorescence (1:100)	Developmental Studies Hybridoma Bank MR1A
phospho- H3(Ser10)	Immunofluorescence (1:1000)	Millipore
pgrp-sc1	AAGCGATCGTCAACTATT	GAGAGCCACTTTGGAAACCA
cec	TGTAAGCTAGTTTATTTCTATGG	GATGAGCCTTTAATGTCC

Fly Genotypes

Clonal analysis was performed with flies of the following genotypes: *hsFLP, UASGFP/X* ; *tubGAL80, neoFRT40A/neoFRT40A* ; *tubGAL4/+* (wild-type), and *hsFLP, UASGFP/X* ; *tubGAL80, neoFRT40A/neoFRT40A* ; *tubGAL4/UASimdCA* (ImdCA positive clones).